ARTICLE | Article in Press

Integrative computational repositioning of Foretinib and PF-03715455 as potential GSTP1 inhibitors for cancer chemosensitization

Marouane Aherkou · Mohammed Hakmi · Yassir Boulaamane · Azeddine Ibrahimi

Received: 9 May 2026 / Accepted: 8 September 2026

Abstract

Glutathione S-transferase P1 (GSTP1) plays a key role in tumor progression and drug detoxification, making it a promising target for reversing chemoresistance in cancer cells. Although several GSTP1 inhibitors have been identified, none have progressed to clinical use, mainly because of low specificity and adverse effects. In this work, we used a virtual screening approach that integrates molecular docking and QSAR modeling to identify, through consensus, new GSTP1 inhibitors among approved and experimental compounds listed in the DrugBank database. PF-03715455 and Foretinib emerged as the most promising candidates among the top-ranked compounds, based on docking scores, predicted pIC_{50} values, and binding free-energy analysis. Molecular dynamics (MD) simulations confirmed that both compounds maintained stable binding conformations and exhibited strong affinity for GSTP1, outperforming the reference inhibitor, TER117. This study presents a novel use of PF-03715455 and reveals a new mechanism for Foretinib, which stabilizes the dynamics essential for GSTP1 function and may prevent substrates from binding to the two active sites, H and G, thereby exerting potent inhibitory effects similar to those of reference inhibitors. This repositioning strategy could reduce costs and accelerate the discovery and development of GSTP1 inhibitors, paving the way for clinical use to improve chemosensitivity in cancer.

Keywords Foretinib · PF-03715455 · GSTP1 · Inhibition · Virtual screening · Machine-learning · Molecular dynamics · Cancer chemoresistance

Introduction

Cancer remains a major global health challenge because of its increasing incidence and high mortality rates. Although important progress has been made in cancer treatment, chemotherapy often fails because of resistance[1]. Chemoresistance limits treatment efficacy by promoting tumor growth and reducing patient survival[2]. As tumors progress, cancer cells activate several cytoprotective and regulatory mechanisms that allow them to resist cytotoxic agents[3].

https://doi.org/10.1038/s41598-026-71327-2

Published online: 16 September 2026

scientific reports

Among the molecular actors involved in these mechanisms, GSTP1 is a cytosolic phase II metabolic enzyme that plays an essential role in cellular detoxification. It catalyzes the conjugation of reduced glutathione (GSH) to electrophilic compounds, thereby facilitating the elimination of toxic substances, including many chemotherapeutic agents[4–8]. In addition to its detoxification function, GSTP1 also plays an important non-enzymatic role in cell survival. It can interact with c-Jun N-terminal kinase (JNK), modulating stress-activated signaling pathways and inhibiting apoptosis[9,10]. GSTP1 overexpression has been widely reported in several cancers and is often associated with reduced drug sensitivity[11]. Therefore, GSTP1 represents an important contributor to cancer chemoresistance, and its inhibition has emerged as a promising strategy to enhance the effectiveness of anticancer treatments[6,12].

GSTP1 is a homodimeric enzyme composed of two identical subunits, each with an active site organized into two functionally distinct regions, including a specific GSH-binding site (G-site) and an adjacent, less specific site (H-site) for hydrophobic electrophilic substrate binding[13–15]. Consequently, GSTP1 inhibitors can act through different binding mechanisms: some preferentially bind the H-site and compete with hydrophobic substrates, while others interact with the G-site, interfering with GSH binding. In some cases, inhibitors may also span both sites, potentially blocking substrate access and disrupting GSTP1's catalytic function[16].

Several compounds, including ethacrynic acid (EA), TER117, and NBDHEX (6-(7-nitro-2,1,3-benzoxadiazol-4-ylthio)hexanol), have shown the ability to inhibit GSTP1 activity and increase the intracellular concentrations of anticancer drugs such as cisplatin and doxorubicin, thereby improving therapeutic efficacy[11,17–19]. However, despite encouraging experimental results, many GSTP1 inhibitors have not progressed to clinical use because of toxicity, limited selectivity, and unfavorable pharmacological properties. In this context, drug repositioning is particularly attractive because it enables the identification of new therapeutic applications for compounds that are already approved or in clinical trials and have known safety profiles and pharmacokinetic characteristics[20–22].

Computer-aided drug discovery represents a valuable strategy for reducing development costs and accelerating the identification of promising GSTP1 inhibitors. Nevertheless, virtual screening based on a single method or scoring function may yield biased results and many false-positive candidates[23–26]. Furthermore, rigid protein models, which do not reflect the natural flexibility of proteins, can reduce the accuracy of binding predictions[27,28].

Based on these considerations, the present study aimed to identify reliable GSTP1 inhibitors using an integrated computational drug-repositioning strategy. To achieve this objective, we used several scoring functions and protein conformations to prioritize candidates by consensus. This approach was designed to improve the reliability of virtual screening results and identify compounds with a high probability of translational success and potential relevance for overcoming cancer chemoresistance.

Materials and methods

Protein and ligand preparations

The human GSTP1 crystal structure complexed with TER117 (PDB ID: 10GS)[29], obtained from the Protein Data Bank, was prepared using Maestro v2025.3's "Protein Preparation Wizard." The process included removing the native ligand, co-crystallized substrates, and waters; assigning bond orders; adding hydrogens; forming disulfide bonds; establishing zero-order bonds to metals; and generating protonation states at pH 7.4 ± 2.0. Small-molecule ligands from the DrugBank database (accessed March 14, 2025) were filtered using Ghose's drug-likeness filter to select 9,185 drug-like compounds with a molecular weight of at least 160 g/mol and at least 10 heavy atoms[30]. We prepared these ligands using Maestro's LigPrep and Epik modules to generate optimized 3D conformations and appropriate ionization states at pH 7.0 ± 2.0[31,32].

Molecular docking

We performed virtual screening on the prepared GSTP1 crystal structure using the Glide module. We centered the binding pocket on key active-site residues at coordinates x = 9.83, y = 6.74, z = 28.12, within a 15 × 15 × 15 Å grid box. Before screening, we validated the docking protocol by redocking the co-crystallized ligand (TER117) to ensure it reproduced the experimental binding pose. The quality of redocking was assessed by calculating the root-mean-square deviation (RMSD) between the experimental and predicted ligand positions, using Glide's superposition tool. RMSD thresholds for interpretation were: < 1 Å (Excellent), 1–2 Å (Good), 2–3 Å (Moderate), and > 3 Å (Poor)[33]. Following validation, all ligands were docked into the GSTP1 active site with Glide's Standard Precision (SP) mode, and their docking scores were employed to rank the ligands based on their predicted binding affinity.

Ensemble rescoring

To improve the accuracy of Glide docking scores, we re-evaluated compounds with scores ≤ −7 kcal/mol using the GSTP1 crystal structure (PDB ID: 10GS) with the same validated parameters. Three docking tools, AutoDock Vina 1.2.5, rDock 0.1.0, and PLANTS 1.2, were used, each with its own scoring algorithm[34–36], to minimize bias from any single software. We also assessed protein flexibility by docking five representative GSTP1 conformations at 1, 25, 50, 75, and 100 ns, extracted from a 100 ns MD simulation with GROMACS v2025.3, following our previous protocol[16]. We converted ligand files to the appropriate formats (pdbqt for AutoDock Vina, mol2 for rDock, and PLANTS) using Open Babel 3.1.1[37].

Machine learning-based QSAR modeling

In addition to molecular docking, we incorporated QSAR analysis to account for ligand physicochemical properties during screening. We trained three machine learning models, Random Forest (RF), Light Gradient-Boosting Machine (LightGBM), and Partial Least Squares (PLS) regression, recognized for their effectiveness with limited or diverse data[38–40], on a dataset of 162 GSTP1 inhibitors from ChEMBL[41]. We split the dataset into 80% for training and 20% for testing. For compounds with multiple IC_{50} values, we averaged them in Pandas to obtain a single representative value and removed duplicates[42]. For each compound, 119 molecular descriptors (Table S1), covering physicochemical properties, ring counts, and topological indices, were calculated using Scikit-Learn[43]. Dimensionality reduction involved removing low-variance descriptors (threshold of 0.01) and highly correlated features (Pearson correlation coefficient > 0.9). Model performance was evaluated via the coefficient of determination (R^2), root mean squared error (RMSE), mean absolute error (MAE), and mean squared error (MSE). We also assessed robustness using leave-one-out (Q^2LOO), 5-fold cross-validation, and Y-scrambling tests to rule out chance correlations. We analyzed the applicability domain with Williams' plot, which combines leverage and residuals to identify influential or unreliable predictions. Leverage values were computed from the hat matrix (H) as follows[44]:

$$H = X(X^T \times X)^{-1} X^T \quad (1)$$

X is the descriptor matrix (n × m), containing n compounds and m descriptors. Its transpose is denoted as X^T. We determined the leverage (h_i) for each compound from this matrix.

$$h_i = x_i^T (X^T \times X)^{-1} \times x_i \quad (2)$$

x_i represents the descriptor row vector for compound i. The warning leverage (h*) is calculated as:

$$h^* = \frac{3 \times (p+1)}{n} \quad (3)$$

Where p represents the number of descriptors and n the number of compounds; compounds with standardized residuals exceeding ± 3 or greater than h* are considered outliers or outside the model's applicability domain.

Consensus ranking

To merge the results from molecular docking and QSAR modeling, we used the exponential consensus ranking (ECR) method[45]. This strategy is employed when each tool produces different rankings for the same compounds[46]. It combines several independent rankings into a single overall ranking, reducing bias from scale differences across approaches. The ECR model assigns greater weight to the highest-ranked molecules via exponential weighting. For each compound i and each scoring function j, an exponential probability score $P(r_i^j)$ was assigned to its ranking r_i^j, calculated as follows:

$$P\left(r_i^j\right) = \frac{1}{\sigma} exp\left(-\frac{r_i^j}{\sigma}\right) \quad (4)$$

Where is a scale parameter that adjusts the influence of the highest-ranked compounds.

We ultimately ranked the molecules based on the average weight assigned to each compound, emphasizing those consistently prioritized by both methods.

Prime MMGBSA

Based on the ECR ranking, we selected the top 50% of compounds to compute the free binding energy ($\Delta G_{binding}$) to GSTP1 using Maestro's Prime MMGBSA module with the OPLS_2005 force field[47]. This approach is used post-docking to provide a more accurate estimate of ligand-protein binding affinity than docking scores, based on the following equation:

$$\Delta G_{Binding} = G_{Complex} - (G_{Protein} + \Delta G_{Ligand}) \quad (5)$$

$G_{Complex}$ indicates the total free energy of the protein-ligand complex, while $G_{protein}$ and G_{ligand} denote the free energies of the protein alone and the ligand alone, respectively. Stronger binding affinities correspond to more negative energy values.

Molecular dynamics simulation

To verify that the previous static results remain stable, realistic, and physically consistent over time, we conducted MD simulations with GROMACS v2025.3 for 500 ns in duplicate to assess trajectory reproducibility[48]. We selected only compounds with notably negative energy values (<- 70 kcal/mol). We built the system models from input files generated by the CHARMM-GUI solution generator, using the CHARMM36m force field[49]. We performed subsequent minimization, equilibration, and trajectory analysis as described in our previous work[16]. Additionally, we used principal component analysis (PCA) and dynamic cross-correlation matrices (DCCM) with the Bio3D package[44] to examine collective movements within the GSTP1 conformational landscape and residue-movement correlations, respectively, revealing how ligand binding affects enzyme dynamics and stability[50]. We used MD-PLIP to profile protein-ligand interactions and characterize the non-covalent interactions established during the MD simulations[51]. We analyzed representative frames from the trajectories to identify the main interaction types, including hydrophobic contacts, hydrogen bonds, π-stacking interactions, and salt bridges. We retained recurrent residues observed across representative frames to define the dominant ligand-binding interaction pattern.

Results

Structure-based virtual screening

Before assessing the binding affinities of the compounds for GSTP1, we validated the docking protocol by re-docking the co-crystallized ligand TER117. Superimposition of the ligand with its redocked pose (Fig. 1) yielded an RMSD of 1.43 Å, well below the 2 Å threshold, confirming the reproducibility of the method. This validation provided a reference binding energy of −7.38 kcal/mol for TER117, which served as a benchmark for later comparisons.

Next, we computed docking scores for 16,112 conformers generated from 9,185 compounds, (Table S2). The results showed a binding energy range for GSTP1 from − 10.33 to + 4.86 kcal/mol, indicating that 87% of ligands have low affinity, 10% moderate affinity, and 3% high affinity. We re-evaluated the top 3% of binders, (360 compounds) with binding energies comparable to or better than TER117, (≤ −7 kcal/mol) using multiple docking tools across different GSTP1 conformations. The rescoring results, (Table S3) showed that some compounds consistently ranked highly across methods and conformations, whereas others varied by software or protein conformation. This variability highlights differences among scoring functions across programs and underscores GSTP1's flexibility, as evidenced by conformations obtained from MD trajectories (Fig. 2).

Ligand-based virtual screening

To improve the reliability of virtual screening for 360 compounds targeting GSTP1, we incorporated QSAR modeling to establish a quantitative relationship between chemical structure and biological activity. Training three regression models (Table 1) showed that RF and LightGBM performed best, with R^2 values of 0.9453 and 0.9136 on the training set, and 0.6451 and 0.59 on the test set, respectively. The PLS model, however, performed less effectively (Fig. S1a), especially on the test set ($R^2 = 0.4286$), suggesting that linear models are less suitable for capturing structure-activity relationships in this dataset. To evaluate model robustness and address potential overfitting issues arising from the performance gap between the training ($R^2 = 0.9453$ for RF) and testing ($R^2 = 0.6451$) datasets, we performed internal validation and applicability domain assessments. Although tree-based ensembles like Random Forest can fit the training set tightly, 5-fold cross-validation ($R^2\_CV = 0.5950$) and leave-one-out validation ($Q^2\_LOO = 0.6165$) confirmed the model's robust predictive power, closely aligned with test performance. The reliability of these predictions was further substantiated by y-scrambling ($R^2\_scramble = -0.1527$), ruling out chance correlations.

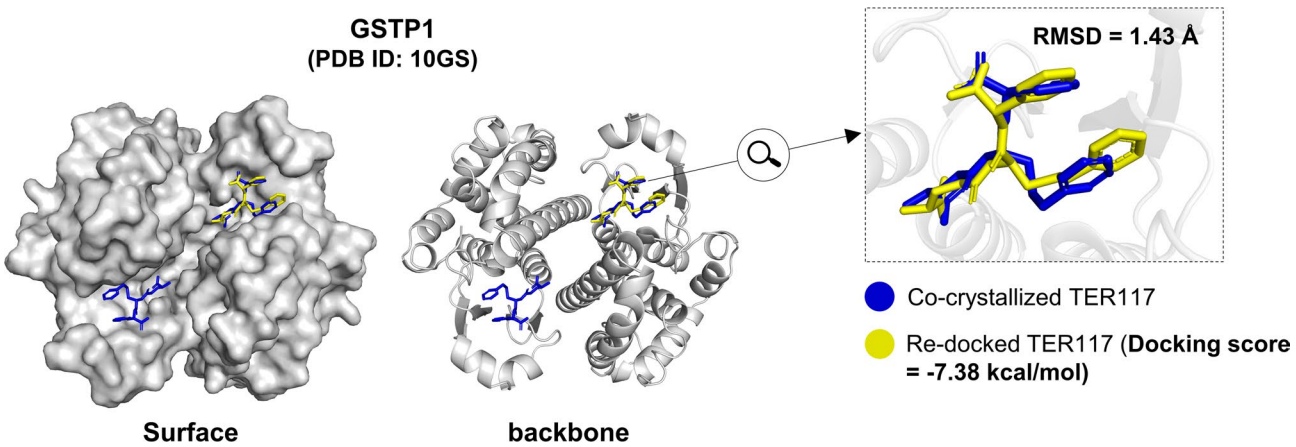

Fig. 1 Superposition of the co-crystallized ligand TER117 pose (blue) and the Glide redocked pose (yellow) in GSTP1, showing an RMSD of 1.43 Å and a docking score of −7.38 kcal/mol.

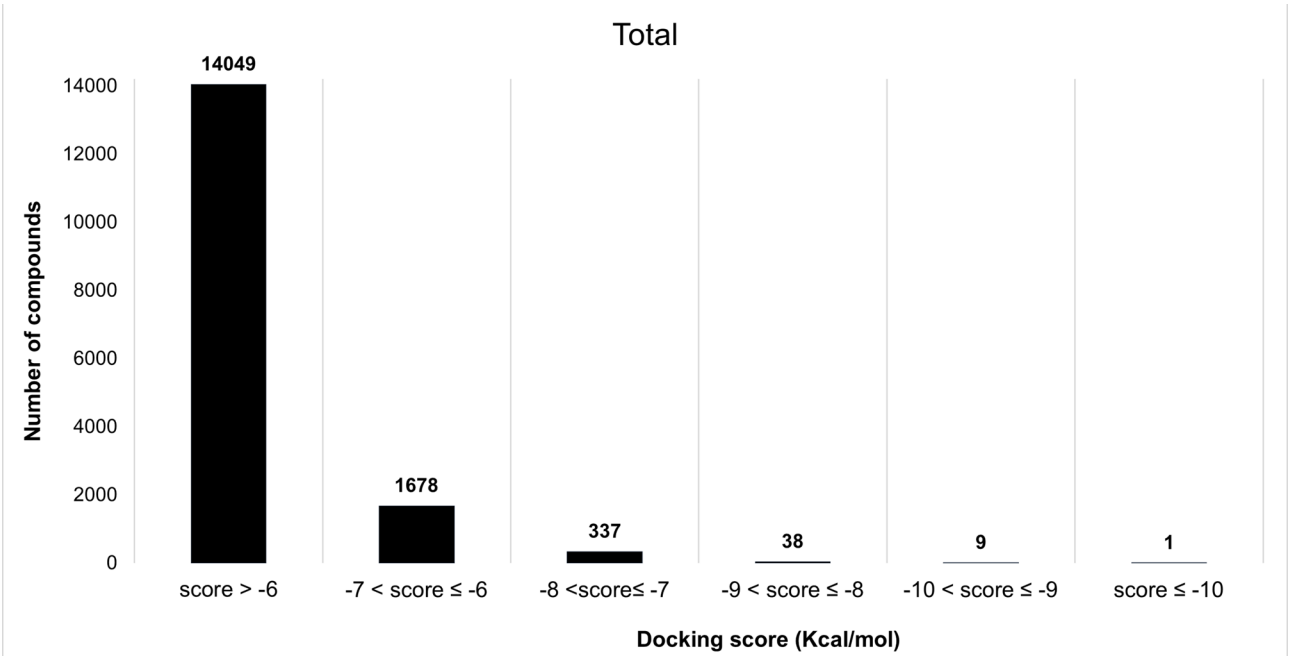

Fig. 2 Distribution of Glide docking scores for 16,112 conformers screened against GSTP1, classified as poor (> −6 kcal/mol), moderate (−7 < score ≤ −6 kcal/mol), or good (≤ −7 kcal/mol).

Table 1 Performance and validation metrics of the RF, LightGBM, and PLS QSAR models.

Dataset		Models		
	Metrics	RF	LightGBM	PLS
Training	R^2	0.9453	0.9136	0.6971
	RMSE	0.2170	0.2728	0.5108
	MAE	0.1558	0.1994	0.4122
	MSE	0.0471	0.0744	0.2609
Test	R^2	0.6451	0.5901	0.4286
	RMSE	0.5371	0.5772	0.6815
	MAE	0.3605	0.3953	0.5047
	MSE	0.2885	0.3332	0.4645
Mean R^2 5-fold CV		0.5950	0.5982	0.4472
Q^2 LOO		0.6165	0.6092	0.4574
R^2 Scramble		−0.1527	−0.2569	−0.4577

Furthermore, the applicability domain mapped via a Williams plot (Fig. S1b), with a warning leverage threshold (h*) of 1.558, showed that the test compounds fell entirely within the leverage boundaries (h < h*) and lay within three standard deviations of the residuals. This confirms that the model generalizes well to structurally diverse chemical scaffolds outside the training environment, without extrapolation errors or a significant loss of predictive confidence.

Analysis of the ten most influential descriptors (Fig. S1c) revealed that RF focuses on ligand chirality and lipophilicity, as indicated by NumStereocenters, SlogP, and peoe_VSA7. Conversely, LightGBM emphasizes electronic surface features and molecular flexibility, using descriptors like peoe_VSA7, SMR, and NumRotatableBonds. PLS mainly relies on MQN-based structural descriptors such as MQN33 and NumSaturatedCarbocycles. Surface-related features, such as FractionCSP3, also play a significant role, underscoring their importance for GSTP1 inhibition. Pairwise comparisons of predicted pIC_{50} values (Fig. S1d) show strong agreement between RF and LightGBM, with results near zero, though PLS predictions diverge more, reflecting lower accuracy and different compound rankings. Overall, these results demonstrate that the RF and LightGBM models met the

performance requirements for reliable predictions, and that the biological activity of the selected compounds (Table S4) can be relied upon to complement the ranking from the previous docking step.

To ensure that the machine-learning-based predictions have chemical and biological validity, we analyzed the mechanistic relevance of the top-performing descriptors with respect to the active-site biochemistry of human GSTP1. The GSTP1 active cleft consists of a polar GSH-binding pocket (G-site) and its adjacent hydrophobic pocket (H-site) that accommodates xenobiotics and inhibitors. Lipophilicity (SlogP) and hydrophobic surface area descriptors (e.g., PEOE_VSA7) are key contributors to model performance, reflecting the importance of hydrophobic interactions and desolvation within the H-site, particularly with residues such as PHE8, VAL10, VAL35, ILE104, and TYR108. Molar refractivity (SMR) quantifies molecular volume and polarizability, indicating the ligand's ability to engage in dispersion forces. In addition, molecular chirality (NumStereocenters) and conformational flexibility (NumRotatableBonds) capture the binding pocket's steric and thermodynamic constraints. The stereoselective nature of GSTP1 favors specific spatial arrangements, while reduced conformational flexibility lowers the entropic penalty upon binding. Together, these descriptors capture the lipophilic, electronic, steric, and thermodynamic properties governing GSTP1 inhibition, providing a clear mechanistic basis for the machine learning models.

Consensus-based ranking

Integrating structure-based and ligand-based approaches for virtual screening to identify new GSTP1 inhibitors revealed notable differences in the rankings of the same compounds (Fig. S2). To improve methodological complementarity, we used consensus ranking, which yields more reliable ligand prioritization and reduces biases introduced by individual methods. Table S5 lists the top compounds using exponential weighting, yielding a combined ranking that integrates docking scores and pIC_{50} values. The $\Delta G_{binding}$ values for 180 highly reliable candidates (top 50%) from the prime MMGBSA post-docking analysis ranged from −83.81 to +7.33 kcal/mol, including 14 compounds with energies ≤ −70 kcal/mol, which are more extreme than that of TER117 (−50.15 kcal/mol).

MD simulation

To evaluate the stability of the chosen systems, we analyzed duplicate 500-ns MD simulation trajectories. We removed three ligands from the simulations because two bind to GSTP1 (GSH analogs), and the third is a radioactive product unsuitable for drug use. As shown in Fig. 3, among the eleven ligands, five exhibited more favorable MM-PBSA binding free energies than the reference compound TER117 (−54.2 ± 7.28 kcal/mol). Notably, DB12138, DB12307, and DB18463 displayed more negative average $\Delta G_{binding}$ values of 69.88 ± 6.2, −68.21 ± 7.02, and −58.84 ± 8.27 kcal/mol, respectively. These stronger binding energies were associated with

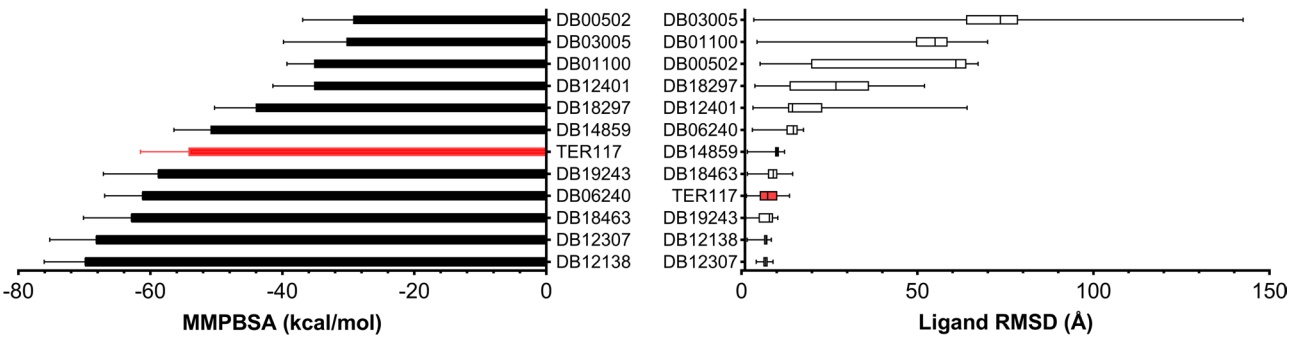

Fig. 3 MM/PBSA binding free energies and ligand RMSD distributions for the GSTP1-ligand complexes during MD simulations (TER117 is highlighted in red).

Table 2 MM/PBSA binding free energy components (kcal/mol) for GSTP1 complexes with the selected hits and the reference ligand TER117.

Values are presented as mean ± SD from two independent MD trajectories.

		Ligand			
		TER117	DB12307	DB19243	DB12138
Energy (Kcal/mol)	$\Delta E_{VDWAALS}$	−72.7 ± 8.3	−92.1 ± 8.1	−90.1 ± 9.7	−106.3 ± 6.6
	ΔE_{EEL}	−51.8 ± 20.4	−162.9 ± 18.6	−54.0 ± 18.6	−21.3 ± 10.3
	ΔE_{EPB}	80.1 ± 20.9	199.1 ± 19.5	97.5 ± 19.4	70.2 ± 13.5
	$\Delta E_{ENPOLAR}$	−9.6 ± 0.7	−12.2 ± 0.8	−12.2 ± 1.0	−12.45 ± 0.4
	ΔE_{GGAS}	−124.6 ± 25.5	−255.0 ± 22.1	−144.1 ± 25.0	−127.7 ± 12.8
	ΔE_{GSOLV}	70.4 ± 20.4	186.8 ± 19.1	78.8 ± 18.7	57.8 ± 13.2
	ΔE_{Total}	−54.2 ± 11.7	−68.2 ± 10.4	−58.8 ± 10.9	−69.8 ± 9.4

Table 3 Key interactions of TER117 and the selected hits with GSTP1 across representative MD simulation frames.

Type	Key residues			
	TER117	DB12307	DB19243	DB12138
Hydrophobic	GLN51, PHE8, VAL35, TRP38, VAL10, ILE104, ILE107	PHE8, PRO9, VAL10, TRP38, ILE104, TYR108, VAL35	PHE8, PRO9, VAL10, VAL35, GLN51, ILE104	PHE8, TYR108, VAL10, VAL35, ARG13, ILE104
H-bond	ARG13, GLN51, GLN64, LEU52, TYR7, TRP38, LYS44, SER65	TYR7, VAL35, ARG13, TRP38, LEU52	LEU52, SER65, GLU97, GLN51, TRP38, GLN64, ASN66	SER105, ILE203, ARG13, TYR108, ASN204
Pi-stacking	PHE8, TYR108	-	PHE8	PHE8, TYR108
Salt bridge	ARG13, LYS44	-	-	-

improved stability within the GSTP1 active site, as reflected by lower ligand RMSD values of 6.7 ± 1.0, 6.8 ± 0.6, and 6.8 ± 2.6 Å for DB12138, DB12307, and DB18463, respectively, compared with TER117 (7.5 ± 2.7 Å). This suggests that the selected ligands remained more stably accommodated in the binding pocket, whereas other compounds showed weaker affinity and instability, including gradual or complete detachment from the active site during simulation.

MM-PBSA analysis showed that van der Waals interactions were the dominant favorable contribution to the binding energies of DB19243 and DB12138, consistent with the energetic profile observed for TER117 (Table 2). This pattern is consistent with non-covalent interactions, mainly recurrent hydrophobic contacts involving PHE8, VAL10, VAL35, and ILE104 (Table 3). DB12138 showed the most favorable van der Waals contribution (−106.3 ± 6.6 kcal/mol). This result was consistent with additional hydrophobic contacts involving ARG13 and TYR108, which appear to play an important role in stabilizing this ligand. For DB12307 and DB19243, the stronger van der Waals contributions (−92.1 ± 8.1 and −90.1 ± 9.7 kcal/mol, respectively), compared with TER117 (−72.7 ± 8.3 kcal/mol), may be explained by hydrophobic contacts involving PRO9, TYR108, and GLN51. Additional aromatic π-stacking interactions were also observed for DB12138 and TER117, involving PHE8 and TYR108.

In contrast, DB12307 showed the most favorable electrostatic contribution, reaching −162.9 ± 18.6 kcal/mol. Interaction analysis revealed hydrogen bonds involving TYR7, VAL35, ARG13, TRP38, and LEU52, as well as hydrophobic contacts with PHE8, PRO9, VAL10, TRP38, ILE104, TYR108, and VAL35. At the same time, the polar desolvation contribution was particularly high for this ligand, reaching + 186.8 ± 19.1 kcal/mol, whereas the corresponding values for the other ligands remained below + 80 kcal/mol.

Overall, these results indicate that TER117, DB19243, and DB12138 exhibited interaction profiles mainly driven by van der Waals contributions and hydrophobic/aromatic contacts, whereas DB12307 displayed an energetic profile more strongly influenced by electrostatic interactions, accompanied by a higher polar desolvation penalty.

The fluctuations in the RMSD of GSTP1 Cα atoms (Fig. 4) indicate that all systems stabilized after about 200 ns. Average RMSDs show that GSTP1 was most structurally stable when bound to DB12307 and DB12138,

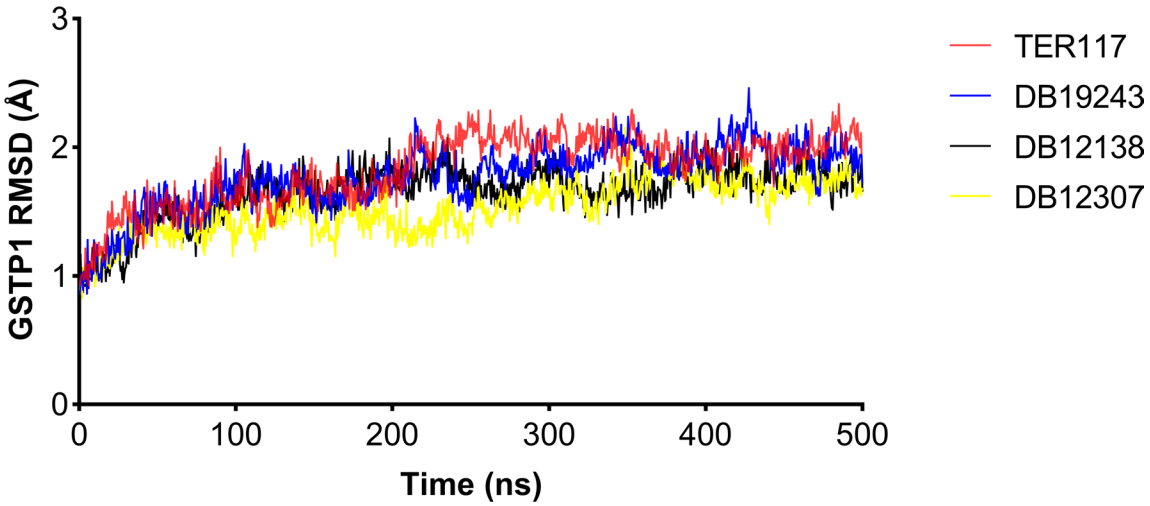

Fig. 4 Time evolution of GSTP1 backbone RMSD during 500-ns MD simulations of the complexes with TER117, DB19243, DB12138, and DB12307.

with RMSDs of 1.53 ± 0.21 Å and 1.65 ± 0.21 Å, respectively. Conversely, the GSTP1-DB19243 complex had a slightly higher average RMSD of 1.77 ± 0.25 Å, although it remained lower than that of TER117 (1.83 ± 0.26 Å).

RMSF analysis of GSTP1 dimer residues (Fig. 5b) confirms that binding of DB12307 and DB12138 stabilizes the enzyme. The secondary structure's flexibility, especially in the C-terminal region (Fig. 5a), was notably altered by these two ligands, whereas it remained flexible with TER117 and DB19243. DCCM analysis (Fig. S3) further showed a significant decrease in intra- and interchain motion correlations within the GSTP1 dimer, indicating a disruption of the protein's natural dynamic coordination. This stabilization is also reflected in the PCA results (Fig. S3), where compounds DB12307 and DB12138 substantially constrained GSTP1's conformational space, accounting for mean variances of 37.9% and 38.7%, respectively. Conversely, DB19243 exhibited greater conformational flexibility, with a captured variance of 42.7%, slightly higher than that of TER117 (41.7%). Overall, these findings suggest that DB12307 and DB12138, corresponding to Foretinib and PF-03715455, exhibit the most stable and energetic profiles, potentially impairing GSTP1 function.

Discussion

Numerous drugs exhibit pleiotropic effects by interacting with multiple molecular pathways, leading to diverse pharmacological outcomes[52]. Researchers have systematically investigated this characteristic in drug repurposing, particularly in oncology[21]. Drug repositioning aims to identify new therapeutic indications for approved or clinically investigated compounds, thereby reducing development timelines, costs, and potential safety risks compared with de novo drug discovery. Several agents, including propranolol (a β-blocker), chloroquine (an antimalarial), and clarithromycin (an antibiotic), originally developed for non-oncological purposes, have demonstrated anticancer activity in experimental models[53–56]. In this context, the present study adopted a computational drug-repositioning strategy to identify novel molecules that may modulate tumor progression and potentially overcome chemoresistance through GSTP1 inhibition.

To improve candidate selection reliability, this study integrated structure-based (SBVS) and ligand-based (LBVS) virtual screening within a consensus workflow[57–59]. This design aimed to overcome the limitations of single-method screening approaches. The selected docking programs employed distinct scoring functions, conformational sampling strategies, and solvation models[60–62], thereby improving ranking robustness and reducing the risk of false-positive selection. In addition, accounting for GSTP1 plasticity was essential, since this enzyme

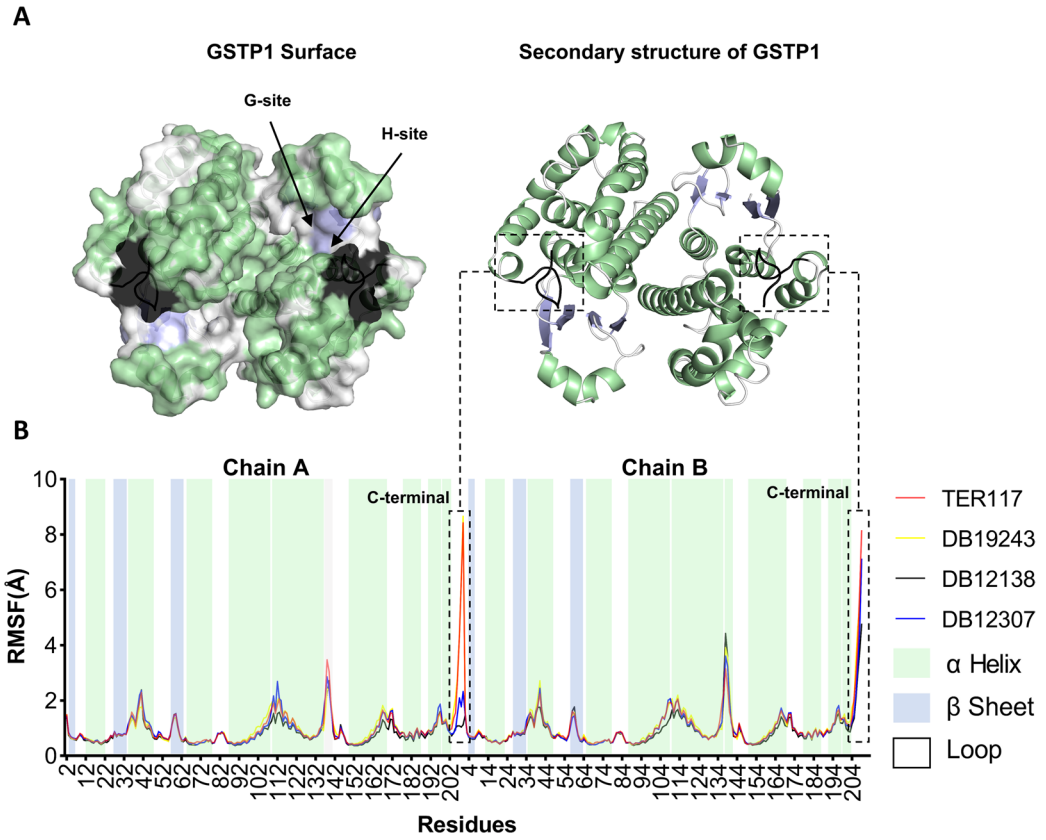

Fig. 5 (**a**) GSTP1 surface showing the G- and H-sites and the corresponding secondary-structure representation. (**b**) Per-residue backbone RMSF profiles of chains A and B for the four GSTP1-ligand complexes; dashed boxes highlight the C-terminal regions.

possesses a highly adaptable active site[27,28]. The flexibility observed during the simulations also supports using multiple receptor conformations rather than relying on a single static structure, as is commonly done in traditional virtual screening protocols[63]. Alongside docking-based prioritization, we used QSAR modeling as a complementary ligand-based filter, a widely used approach to improve the credibility of virtual screening campaigns[64]. Our results are consistent with previous GSTP1-1-focused QSAR findings reported by Almi et al.[65], who showed that a non-linear model outperformed a linear model in predicting GSTP1-1 inhibition from molecular descriptors. This suggests that the relationship between molecular descriptors and GSTP1 inhibitory activity is likely non-linear. However, their study was mainly limited to nitrobenzoxadiazole derivatives. In contrast, the present study extends this concept by using a chemically more diverse set of GSTP1 inhibitors and by comparing recent machine-learning models, including Random Forest and LightGBM, thereby improving candidate selection and providing additional insight into the relationship between chemical structure and predicted biological activity[66]. Because compounds outside the applicability domain may increase the false-positive rate, we applied a strict applicability-domain filter to retain only candidates within the high-confidence region of chemical space. The ECR score assigned to each compound further integrated results from multiple scoring functions[45], yielding a more effective ranking than single-score prioritization strategies[67–69].

This integrative strategy identified two molecules, not previously reported as GSTP1 inhibitors, as promising computational candidates for GSTP1 inhibition. PF-03715455, a p38α MAPK inhibitor, was initially developed for asthma and chronic obstructive pulmonary disease in phase 2 clinical trials[70–72] and has also been evaluated for other indications, including SARS-CoV-2 and inflammatory diseases[73–75]. Foretinib, a multi-kinase inhibitor

initially developed as an anticancer agent, was also identified as a promising hit, suggesting a potential additional mechanism of action through GSTP1 targeting.

MD simulations using the GSTP1 dimer provided a more physiologically relevant representation of the enzyme than monomer-based models, since GSTP1 functions as an active homodimer[13]. The simulations indicated stable binding of PF-03715455 and Foretinib to GSTP1, as reflected by RMSD values. Enzyme flexibility is critical to GSTP1 function[76,77], and RMSF analysis suggests that ligand binding may reduce flexibility, particularly in the C-terminal region, which is essential for substrate access to the active site[78]. Human GSTP1 functions as a homodimer, with each subunit containing a GSH-binding site (G-site) and an adjacent hydrophobic site (H-site) that accommodates various xenobiotics[14,15]. Therefore, stable ligand occupancy within these subsites may interfere with substrate recognition and catalytic pocket organization.

MM-PBSA analysis revealed that PF-03715455 primarily engages GSTP1 through van der Waals contributions, indicating a molecular recognition mode largely dominated by hydrophobic interactions. This observation is consistent with the ligand's physicochemical properties, which favor accommodation within hydrophobic environments[79,80]. Compared with EA-GSH, PF-03715455 therefore appears to rely more strongly on hydrophobic and aromatic stabilization. Its highly favorable van der Waals contribution, together with recurrent contacts involving PHE8, VAL10, VAL35, ILE104, and TYR108, suggests preferential anchoring within the H-site. Additional contacts involving ARG13 and TYR108 may further explain the marked stability of this ligand, particularly since TYR108 is located in a region that contributes to ligand accommodation and catalytic pocket organization. Moreover, the relatively rigid structure of PF-03715455 may favor optimal steric complementarity with the H-site, allowing stable positioning within the pocket[81,82]. The involvement of key residues such as PHE8, ILE104, and TYR108 is particularly relevant, as these residues may obstruct the H-site and limit substrate access[83–85]. In addition, π-stacking interactions with PHE8 and TYR108 may reinforce ligand stabilization and help maintain its binding pose during the simulation. Thus, PF-03715455 appears to partially mimic the spatial occupation previously observed for EA-GSH[16], while adopting a binding mechanism more strongly driven by hydrophobic/aromatic anchoring.

In contrast, Foretinib displayed a more electrostatically driven profile. Its strong electrostatic contribution is consistent with hydrogen bonds involving TYR7, ARG13, VAL35, TRP38, and LEU52, several of which are located near or at the interface between the G-site and H-site. This interaction pattern suggests that Foretinib may behave as a dual-site ligand, combining polar interactions near the G-site with hydrophobic contacts involving PHE8, PRO9, VAL10, TRP38, ILE104, TYR108, and VAL35. However, the highly favorable electrostatic contribution was accompanied by a substantial polar desolvation penalty, indicating that ligand binding requires an energetic cost associated with desolvating polar groups. This compensation between electrostatic attraction and polar desolvation is commonly observed for ligands that form multiple polar contacts within protein-binding pockets. Therefore, although Foretinib benefits from strong hydrogen bonding and electrostatic interactions, its final binding stability likely results from a balance between favorable polar contacts and unfavorable desolvation effects.

Overall, the comparison with EA-GSH and TER117 suggests that the most relevant feature of these new hits is their ability to engage residues from both the G-site and the H-site, albeit through distinct energetic mechanisms. PF-03715455 appears to adopt mainly a hydrophobic/aromatic anchoring mechanism, favored by its compatibility with the H-site, whereas Foretinib behaves more as a dual-site ligand with a stronger polar character. This simultaneous or extended occupation of both subsites may be important for GSTP1 inhibition, as it could limit substrate access, interfere with glutathione-related recognition, and disturb the functional organization of the catalytic pocket. These findings support the potential of the identified hits as GSTP1 inhibitors, with interaction profiles that differ from but partially overlap those of the reference inhibitors.

These findings are particularly relevant when compared with previous GSTP1-targeting strategies. Pseudosubstrates targeting GSTP1's G-site, such as Canfosfamide and Ezatiostat, have not achieved sufficient clinical efficacy for standard oncology applications[86–91]. This limitation may stem from interference with GSH metabolism, which is essential for normal cellular function and may contribute to toxicity and limited tolerability. In

contrast, although development of PF-03715455 was discontinued for economic reasons, available clinical data have not highlighted major toxicity concerns[92], suggesting that it may represent a safer repositioning candidate.

Foretinib, an experimental agent with recognized anticancer properties[86], has been evaluated in phase 2 clinical trials for its ability to inhibit angiogenesis and tumor growth by targeting multiple kinases, including c-MET, VEGFR2, RON, and Axl[93–96]. Although multi-kinase inhibition is important, kinase expression varies among tumors and is often restricted to specific subgroups, which can affect clinical efficacy and contribute to toxicities resulting from inhibition of essential physiological pathways[87–89]. In contrast, GSTP1 is widely overexpressed in many cancers, independently of mutation status[90]. Thus, the present study proposes a novel and potentially relevant mechanism of action for foretinib through GSTP1 targeting. Its energetic behavior, which partially resembles that of EA-GSH[91], is also supported by LBVS hypotheses emphasizing the compound's semi-rigid structure and electrostatic surface[97]. Additionally, the structural stabilization induced by foretinib, as indicated by RMSF, DCCM, and PCA analyses, appears stronger than that reported in the fosaprepitant repositioning study[98], suggesting a potential inhibitory effect.

From a biological perspective, the anticipated inhibition of GSTP1 by PF-03715455 and foretinib is particularly important, as GSTP1 contributes to chemoresistance through glutathione-dependent detoxification of electrophilic anticancer agents, attenuation of oxidative stress, and modulation of apoptosis-related signaling pathways[4–8]. Consequently, stable occupancy of the GSTP1 active site, along with reduced flexibility, could impair substrate recognition and reduce tumor cells' detoxification capacity, potentially restoring sensitivity to cytotoxic chemotherapy[16]. Furthermore, compounds that restrict GSTP1 conformational dynamics may interfere not only with substrate detoxification but also with non-catalytic regulatory functions involved in tumor cell survival, particularly by disrupting GSTP1-mediated inhibition of JNK signaling and promoting apoptosis reactivation[9,10].

In summary, PF-03715455 and foretinib emerge as promising computational candidates for GSTP1 inhibition and drug repositioning. These compounds merit further experimental evaluation to confirm their GSTP1 inhibitory activity and evaluate their potential effects on tumor progression and chemoresistance.

Conclusion

The findings indicate that integrating LBVS and SBVS strengthens GSTP1 inhibitor identification by combining complementary ligand- and structure-based criteria. Molecular docking, QSAR modeling, MD simulations, and MM/PBSA calculations consistently identified PF-03715455 and foretinib as promising candidates with stable binding profiles and the potential to influence GSTP1 structural and dynamic properties critical to its function. Nevertheless, the current study has limitations, primarily related to the size and chemical diversity of the dataset used to train the QSAR models. Expanding this dataset would improve model generalizability and broaden its applicability domain. Furthermore, screening larger and more diverse molecular libraries would enable broader exploration of chemical space and could reveal additional promising GSTP1-targeting scaffolds. Finally, these computational predictions require experimental validation to confirm the inhibitory activities of the selected compounds. Future studies should therefore include GSTP1 enzymatic inhibition assays, evaluation of cytotoxicity and chemosensitizing effects in a GSTP1-overexpressing cancer cell line, and further structure-activity optimization of the most promising scaffolds. Overall, this drug-repositioning strategy could accelerate the development of GSTP1-targeted therapies to overcome chemoresistance. With appropriate experimental and preclinical validation, this approach may ultimately contribute to more effective treatment options for patients with cancer.

Supplementary Information The online version contains supplementary material available at https://doi.org/10.1038/s41598-026-71327-2.

Author contributions M.A.: conceptualization, investigation, writing – original draft, methodology, software, formal analysis. M.H.: investigation, validation, software, writing – review and editing, formal analysis. Y.B.: investigation, software,

writing – review and editing. A.I.: supervision, project administration, resources, writing – review and editing, validation. All authors read and approved the final manuscript.

Funding This study had no specific funding sources.

Data availability The data is available upon request at: https://doi.org/10.5281/zenodo.18875963 All data are included in the manuscripts and supporting information. Molecular docking protocols were performed using the Glide module in the Schrödinger Suite (version 2025.3), downloaded from https://my.schrodinger.com/download/software/. Additional docking programs include AutoDock Vina 1.2.5, rDock 0.1.0, and PLANTS 1.2, all of which are freely available online. Molecular dynamics simulations were performed using GROMACS (2025.3).

Declarations

Competing interests The authors declare no competing interests.

References

1. Bukowski, K., Kciuk, M. & Kontek, R. Mechanisms of multidrug resistance in cancer chemotherapy. *Int. J. Mol. Sci.* **21**(9), 3233. https://doi.org/10.3390/IJMS21093233 (2020).
2. Kar, A., Agarwal, S., Singh, A., Bajaj, A. & Dasgupta, U. Insights into molecular mechanisms of chemotherapy resistance in cancer. *Transl. Oncol.* **42**, 101901. https://doi.org/10.1016/J.TRANON.2024.101901 (2024).
3. Cui, J. et al. GSTP1 and cancer: Expression, methylation, polymorphisms and signaling (Review). *Int. J. Oncol.* **56** (4), 867–878. https://doi.org/10.3892/ijo.2020.4979 (2020).
4. Singh, R. R. & Reindl, K. M. Glutathione S-transferases in cancer. *Antioxidants* **10**, 701. https://doi.org/10.3390/ANTIOX10050701 (2021).
5. Chatterjee, A. & Gupta, S. The multifaceted role of glutathione S-transferases in cancer. *Cancer Lett.* **433**, 33–42. https://doi.org/10.1016/J.CANLET.2018.06.028 (2018).
6. Pljesa-Ercegovac, M. et al. Glutathione transferases: Potential targets to overcome chemoresistance in solid tumors. *Int. J. Mol. Sci.* **19**(12), 3785. https://doi.org/10.3390/IJMS19123785 (2018).
7. Singh, S. Cytoprotective and regulatory functions of glutathione S-transferases in cancer cell proliferation and cell death. *Cancer Chemother. Pharmacol.* **75**(1), 1–15. https://doi.org/10.1007/S00280-014-2566-X/METRICS (2015).
8. Mazari, A. M. A. et al. The multifaceted role of glutathione S-transferases in health and disease. *Biomolecules* **13**(4), 688. https://doi.org/10.3390/BIOM13040688 (2023).
9. Adler, V. et al. Regulation of JNK signaling by GSTp. *EMBO J.* **18**(5), 1321–1334. https://doi.org/10.1093/EMBOJ/18.5.1321 (1999).
10. Townsend, D. M. & Tew, K. D. The role of glutathione-S-transferase in anti-cancer drug resistance. *Oncogene* **22**(47), 7369–7375. https://doi.org/10.1038/sj.onc.1206940 (2003).
11. Lv, N. et al. Overexpression of glutathione S-transferases in human diseases: Drug targets and therapeutic implications. *Antioxidants*. https://doi.org/10.3390/antiox12111970 (2023).
12. Al-Najjar, B. O., Helal, M., Saqallah, F. G. & Bandy, B. Isozyme-specific inhibition of GSTP1-1: A crucial element in cancer-targeting drugs. *RSC Med. Chem.* https://doi.org/10.1039/D4MD00872C (2025).
13. Wu, B. & Dong, D. Human cytosolic glutathione transferases: Structure, function, and drug discovery. *Trends Pharmacol. Sci.* **33**(12), 656–668. https://doi.org/10.1016/j.tips.2012.09.007 (2012).
14. Oakley, A. Glutathione transferases: A structural perspective. *Drug Metab. Rev.* **43**(2), 138–151. https://doi.org/10.3109/03602532.2011.558093 (2011).

15. Oakley, A. J. et al. The three-dimensional structure of the human pi class glutathione transferase P1-1 in complex with the inhibitor ethacrynic acid and its glutathione conjugate. *Biochemistry* **36**(3), 576–585. https://doi.org/10.1021/BI962316I (1997).
16. Aherkou, M., Hakmi, M., Bouricha, E. M., Belyamani, L. & Ibrahimi, A. Deciphering glutathione S-transferase P1 inhibition mechanisms for overcoming cancer chemoresistance: Insights from computational analysis. *Proteins Struct. Funct. Bioinforma.* https://doi.org/10.1002/PROT.70093 (2025).
17. Awasthi, S. et al. Modulation of doxorubicin cytotoxicity by ethacrynic acid. *Int. J. Cancer* **68**(3), 333–339 (1996).
18. Rhodes, T. & Twentyman, P. R. A study of ethacrynic acid as a potential modifier of melphalan and cisplatin sensitivity in human lung cancer parental and drug-resistant cell lines. *Br. J. Cancer*. **65** (5), 684–690 (1992).
19. Lyttle, M. H. et al. Isoenzyme-specific glutathione-S-transferase inhibitors: Design and synthesis. *J. Med. Chem.* **37**(1), 189–194. https://doi.org/10.1021/JM00027A024 (1994).
20. Lin, H. et al. Identification of fosaprepitant as a novel GSTP1 inhibitor through structure-based virtual screening, molecular dynamics simulation, and biological evaluation. *New J. Chem.* **46**(3), 1042–1053. https://doi.org/10.1039/D1NJ04597K (2022).
21. Pantziarka, P., Verbaanderd, C., Huys, I., Bouche, G. & Meheus, L. Repurposing drugs in oncology: From candidate selection to clinical adoption. *Semin Cancer Biol.* **68**, 186–191. https://doi.org/10.1016/J.SEMCANCER.2020.01.008 (2021).
22. Pushpakom, S. et al. Drug repurposing: Progress, challenges and recommendations. *Nat. Rev. Drug Discov*. **18** (1), 41–58. https://doi.org/10.1038/nrd.2018.168 (2018).
23. Chaput, L., Martinez-Sanz, J., Saettel, N. & Mouawad, L. Benchmark of four popular virtual screening programs: construction of the active/decoy dataset remains a major determinant of measured performance. *J. Cheminform* **8**(1), 1–17. https://doi.org/10.1186/S13321-016-0167-X/FIGURES/7 (2016).
24. Cross, J. B. et al. Comparison of several molecular docking programs: Pose prediction and virtual screening accuracy. *J. Chem. Inf. Model.* **49**(6), 1455–1474. https://doi.org/10.1021/CI900056C/SUPPL_FILE/CI900056C_SI_001.PDF (2009).
25. Li, X., Li, Y., Cheng, T., Liu, Z. & Wang, R. Evaluation of the performance of four molecular docking programs on a diverse set of protein-ligand complexes. *J. Comput. Chem.* **31**(11), 2109–2125. https://doi.org/10.1002/JCC.21498;PAGE:STRING:ARTICLE/CHAPTER (2010).
26. Wang, Z. et al. Comprehensive evaluation of ten docking programs on a diverse set of protein–ligand complexes: The prediction accuracy of sampling power and scoring power. *Phys. Chem. Chem. Phys.* **18**(18), 12964–12975. https://doi.org/10.1039/C6CP01555G (2016).
27. Totrov, M. & Abagyan, R. Flexible ligand docking to multiple receptor conformations: a practical alternative. *Curr. Opin. Struct. Biol.* **18**(2), 178–184. https://doi.org/10.1016/J.SBI.2008.01.004 (2008).
28. Bottegoni, G., Rocchia, W., Rueda, M., Abagyan, R. & Cavalli, A. Systematic exploitation of multiple receptor conformations for virtual ligand screening. *PLoS One* **6**(5), e18845. https://doi.org/10.1371/JOURNAL.PONE.0018845 (2011).
29. Oakley, A. J. et al. The structures of human glutathione transferase P1-1 in complex with glutathione and various inhibitors at high resolution. *J. Mol. Biol.* **274**(1), 84–100. https://doi.org/10.1006/JMBI.1997.1364 (1997).
30. Ghose, A. K., Viswanadhan, V. N. & Wendoloski, J. J. A knowledge-based approach in designing combinatorial or medicinal chemistry libraries for drug discovery. 1. A qualitative and quantitative characterization of known drug databases. *J. Comb. Chem.* **1**(1), 55–68. https://doi.org/10.1021/CC9800071 (1998).
31. Madhavi Sastry, G., Adzhigirey, M., Day, T., Annabhimoju, R. & Sherman, W. Protein and ligand preparation: Parameters, protocols, and influence on virtual screening enrichments. *J. Comput. Mol. Des.* **27**(3), 221–234. https://doi.org/10.1007/S10822-013-9644-8 (2013).
32. Shelley, J. C. et al. Epik: A software program for pK a prediction and protonation state generation for drug-like molecules. *J. Comput. Mol. Des.* **21**(12), 681–691. https://doi.org/10.1007/S10822-007-9133-Z (2007).
33. Mateev, E., Valkova, I., Angelov, B., Georgieva, M. & Zlatkov, A. Validation through re-docking, cross-docking and ligand enrichment in various well-resoluted Mao-B receptors. *Int. J. Pharm. Sci. Res.* **13**(3), 1099. https://doi.org/10.13040/IJPSR.0975-8232.13 (2022).
34. Trott, O. & Olson, A. J. AutoDock Vina: Improving the speed and accuracy of docking with a new scoring function, efficient optimization, and multithreading. *J. Comput. Chem.* **31**(2), 455–461. https://doi.org/10.1002/JCC.21334 (2010).
35. Ruiz-Carmona, S. et al. rDock: A fast, versatile and open source program for docking ligands to proteins and nucleic acids. *PLoS Comput. Biol.* **10**(4), 1–7. https://doi.org/10.1371/journal.pcbi.1003571 (2014).
36. Korb, O., Stützle, T. & Exner, T. E. Application of ant colony optimization to structure-based drug design. *EMBO J.* **4150**, 247–258. https://doi.org/10.1007/11839088_22 (2006).
37. O'Boyle, N. M. et al. Open Babel: An open chemical toolbox. *J. Cheminform.* **3**(33), 1–14. https://doi.org/10.1186/1758-2946-3-33 (2011).
38. Stawiski, M., Meier, P., Dornberger, R. & Hanne, T. Using the light gradient boosting machine for prediction in QSAR models. *EMBO J.* https://doi.org/10.1007/978-981-99-1435-7_10 (2023).

39. Svetnik, V. et al. Random Forest: A classification and regression tool for compound classification and QSAR modeling. *J. Chem. Inf. Comput. Sci.* **43**(6), 1947–1958. https://doi.org/10.1021/CI034160G/SUPPL_FILE/CI034160GSI20031008_041202.ZIP (2003).
40. Olah, M., Bologa, C. & Oprea, T. I. An automated PLS search for biologically relevant QSAR descriptors. *J. Comput. Aided Mol. Des.* **18**, 7–9. https://doi.org/10.1007/S10822-004-4060-8/METRICS (2004).
41. Gaulton, A. et al. ChEMBL: A large-scale bioactivity database for drug discovery. *Nucleic Acids Res.* **40**(D1), D1100–D1107. https://doi.org/10.1093/NAR/GKR777 (2012).
42. Mckinney, W. pandas: a Foundational Python Library for Data Analysis and Statistics, in *Python for high performance and scientific computing*, 1–9. (accessed Jan 12 2026). (2011). http://pandas.sf.net
43. Pedregosa, F. et al. Scikit-learn: Machine learning in Python. *J. Mach. Learn. Res.* **12**, 2825–2830 (2011).
44. Gramatica, P. Principles of QSAR models validation: Internal and external. *QSAR Comb. Sci* **26**(5), 694–701. https://doi.org/10.1002/QSAR.200610151;WGROUP:STRING:PUBLICATION (2007).
45. Palacio-Rodríguez, K., Lans, I., Cavasotto, C. N. & Cossio, P. Exponential consensus ranking improves the outcome in docking and receptor ensemble docking. *Sci. Rep.* **9** (1), 1–14. https://doi.org/10.1038/s41598-019-41594-3 (2019).
46. Blanes-Mira, C. et al. Comprehensive survey of consensus docking for high-throughput virtual screening. *Molecules* https://doi.org/10.3390/molecules28010175 (2023).
47. Wang, E. et al. End-point binding free energy calculation with MM/PBSA and MM/GBSA: Strategies and applications in drug design. *Chem. Rev.* **119**(16), 9478–9508. https://doi.org/10.1021/ACS.CHEMREV.9B00055 (2019).
48. Berendsen, H. J. C., van der Spoel, D. & van Drunen, R. GROMACS: A message-passing parallel molecular dynamics implementation. *Comput. Phys. Commun.* **91**(1–3), 43–56. https://doi.org/10.1016/0010-4655(95)00042-E (1995).
49. Huang, J. et al. CHARMM36m: An improved force field for folded and intrinsically disordered proteins. *Nat. Methods* **14**(1), 71–73. https://doi.org/10.1038/nmeth.4067 (2016).
50. Kitao, A. Principal component analysis and related methods for investigating the dynamics of biological macromolecules. *J — Multidiscip. Sci. J.* **5**(2), 298–317. https://doi.org/10.3390/J5020021 (2022).
51. Schake, P., Bolz, S. N., Linnemann, K. & Schroeder, M. PLIP 2025: Introducing protein–protein interactions to the protein–ligand interaction profiler. *Nucleic Acids Res.* **53**(W1), W463–W465. https://doi.org/10.1093/NAR/GKAF361 (2025).
52. Giordano, S. & Petrelli, A. From single- to multi-target drugs in cancer therapy: When aspecificity becomes an advantage. *Curr. Med. Chem.* **15**(5), 422–432. https://doi.org/10.2174/092986708783503212 (2008).
53. Pantziarka, P. et al. ReDO_DB: the repurposing drugs in oncology database. *Ecancermedicalscience* **12**, 886. https://doi.org/10.3332/ECANCER.2018.886 (2018).
54. Pantziarka, P. et al. Repurposing Drugs in Oncology (ReDO)—Propranolol as an anti-cancer agent. *Ecancermedicalscience* **10**, 680. https://doi.org/10.3332/ECANCER.2016.680 (2016).
55. Verbaanderd, C. et al. Repurposing Drugs in Oncology (ReDO)—chloroquine and hydroxychloroquine as anti-cancer agents. *Ecancermedicalscience* **11**, 781. https://doi.org/10.3332/ECANCER.2017.781 (2017).
56. Van Nuffel, A. M. T. et al. Repurposing Drugs in Oncology (ReDO)—clarithromycin as an anti-cancer agent. *Ecancermedicalscience* **9**, 513. https://doi.org/10.3332/ECANCER.2015.513 (2015).
57. Bhunia, S. S., Saxena, M. & Saxena, A. K. Ligand- and structure-based virtual screening in drug discovery. *Top. Med. Chem.* **37**, 281–339. https://doi.org/10.1007/7355_2021_130 (2021).
58. Dixit, A. & Verkhivker, G. M. Integrating ligand-based and protein-centric virtual screening of kinase inhibitors using ensembles of multiple protein kinase genes and conformations. *J. Chem. Inf. Model.* **52**(10), 2501–2515. https://doi.org/10.1021/CI3002638/ASSET (2012).
59. Mahajan, P. et al. Discovery of novel small molecule EGFR inhibitory leads by structure and ligand-based virtual screening. *Med. Chem. Res.* **26**(1), 74–92. https://doi.org/10.1007/S00044-016-1728-2/METRICS (2017).
60. Liu, J. & Wang, R. Classification of current scoring functions. *J. Chem. Inf. Model.* **55**(3), 475–482. https://doi.org/10.1021/CI500731A/ASSET/IMAGES/MEDIUM/CI-2014-00731A_0003.GIF (2015).
61. Kearsley, S. K., Underwood, D. J., Sheridan, R. P. & Miller, M. D. Flexibases: A way to enhance the use of molecular docking methods. *J. Comput. Aided. Mol. Des.* **8**(5), 565–582. https://doi.org/10.1007/BF00123666/METRICS (1994).
62. Goodsell, D. S., Morris, G. M. & Olson, A. J. Automated docking of flexible ligands: Applications of autodock. *J. Mol. Recognit.* **9**(1), 1–5 (1996).
63. Perola, E. Minimizing false positives in kinase virtual screens. *Proteins Struct. Funct. Bioinforma.* **64**(2), 422–435. https://doi.org/10.1002/PROT.21002 (2006).
64. Shelke, S. et al. Integrated QSAR, molecular docking, and dynamics-based discovery of a potent selective HDAC1 inhibitor with therapeutic potential in aggressive cancers. *J. Mol. Graph. Model.* **143**, 109271. https://doi.org/10.1016/J.JMGM.2025.109271 (2026).
65. Almi, I. et al. QSAR investigations and structure-based virtual screening on a series of nitrobenzoxadiazole derivatives targeting human glutathione-S-transferases. *J. Mol. Struct.* **1211**, 128015. https://doi.org/10.1016/J.MOLSTRUC.2020.128015 (2020).

66. Matveieva, M. & Polishchuk, P. Benchmarks for interpretation of QSAR models. *J. Cheminform* **13**(1), 1–20. https://doi.org/10.1186/S13321-021-00519-X/FIGURES/11 (2021).
67. Wang, R. & Wang, S. How does consensus scoring work for virtual library screening? An idealized computer experiment. *J. Chem. Inf. Comput. Sci.* **41**, 3–6. https://doi.org/10.1021/CI010025X;WGROUP:STRING:ACHS (2001).
68. Oda, A., Tsuchida, K., Takakura, T., Yamaotsu, N. & Hirono, S. Comparison of consensus scoring strategies for evaluating computational models of protein-ligand complexes. *J. Chem. Inf. Model.* **46** (1), 380–391. https://doi.org/10.1021/CI050283K/SUPPL_FILE/CI050283KSI20050913_045539.PDF (2006).
69. Chilingaryan, G. et al. Combination of consensus and ensemble docking strategies for the discovery of human dihydroorotate dehydrogenase inhibitors. *Sci. Rep.* **11**(1), 1–11. https://doi.org/10.1038/s41598-021-91069-7 (2021).
70. Madkour, M. M., Anbar, H. S. & El-Gamal, M. I. Current status and future prospects of p38α/MAPK14 kinase and its inhibitors. *Eur. J. Med. Chem.* **213**, 113216. https://doi.org/10.1016/J.EJMECH.2021.113216 (2021).
71. Pasqua, E., Hamblin, N., Edwards, C., Baker-Glenn, C. & Hurley, C. Developing inhaled drugs for respiratory diseases: A medicinal chemistry perspective. *Drug Discov. Today* **27**(1), 134–150. https://doi.org/10.1016/J.DRUDIS.2021.09.005 (2022).
72. Singh, D. et al. Oral and inhaled p38 MAPK inhibitors: effects on inhaled LPS challenge in healthy subjects. *Eur. J. Clin. Pharmacol.* **71**(10), 1175–1184. https://doi.org/10.1007/S00228-015-1920-1 (2015).
73. El Aissouq, A., Chedadi, O., Bouachrine, M. & Ouammou, A. Identification of novel SARS-CoV-2 inhibitors: A structure-based virtual screening approach. *J. Chem.* **2021**(1), 1901484. https://doi.org/10.1155/2021/1901484 (2021).
74. Romeo, I. et al. Targeting SARS-CoV-2 nsp13 helicase and assessment of druggability pockets: Identification of two potent inhibitors by a multi-site in silico drug repurposing approach. *Molecules* **27**(21), 7522. https://doi.org/10.3390/MOLECULES27217522/S1 (2022).
75. Yu, H. et al. Safety and efficacy of p38 mitogen-activated protein kinase inhibitors (MAPKIs) in COPD. *Front. Pharmacol.* **13**, 950035. https://doi.org/10.3389/FPHAR.2022.950035/FULL (2022).
76. Kokkinidis, M., Glykos, N. M. & Fadouloglou, V. E. Protein flexibility and enzymatic catalysis. *Adv. Protein Chem. Struct. Biol.* **87**, 181–218. https://doi.org/10.1016/B978-0-12-398312-1.00007-X (2012).
77. Kamerlin, S. C. L. & Warshel, A. At the dawn of the 21st century: Is dynamics the missing link for understanding enzyme catalysis?. *Proteins Struct. Funct. Bioinforma.* **78**(6), 1339–1375. https://doi.org/10.1002/PROT.22654 (2010).
78. Tew, K. D. et al. The role of glutathione S-transferase P in signaling pathways and S-glutathionylation in cancer. *Free Radic. Biol. Med.* **51**(2), 299–313. https://doi.org/10.1016/J.FREERADBIOMED.2011.04.013 (2011).
79. Suaifan, G. A. R. Y., Shehadehh, M., Al-Ijel, H. & Taha, M. O. Extensive ligand-based modeling and in silico screening reveal nanomolar inducible nitric oxide synthase (iNOS) inhibitors. *J. Mol. Graph. Model.* **37**, 1–26. https://doi.org/10.1016/J.JMGM.2012.04.001 (2012).
80. Yang, J. F. et al. CIPDB: A biological structure databank for studying cation and π interactions. *Drug Discov. Today* **28**(5), 103546. https://doi.org/10.1016/J.DRUDIS.2023.103546 (2023).
81. Mandal, D. K. Stereochemical concepts. *Pericyclic Chem.* https://doi.org/10.1016/B978-0-12-814958-4.00002-7 (2018).
82. Del Bello, F. et al. Mode of interaction of 1,4-dioxane agonists at the M2 and M3 muscarinic receptor orthosteric sites. *Bioorg. Med. Chem. Lett.* **24**(15), 3255–3259. https://doi.org/10.1016/J.BMCL.2014.06.020 (2014).
83. Zimniak, P. et al. Naturally occurring human glutathione S-transferase GSTP1-1 isoforms with isoleucine and valine in position 104 differ in enzymic properties. *Eur. J. Biochem.* **224**(3), 893–899. https://doi.org/10.1111/J.1432-1033 (1994).
84. Federici, L. et al. Structural basis for the binding of the anticancer compound 6-(7-nitro-2,1,3-benzoxadiazol-4-ylthio) hexanol to human glutathione S-transferases. *Cancer Res.* **69**(20), 8025–8034 (2009).
85. Lo Bello, M. et al. Multifunctional role of Tyr 108 in the catalytic mechanism of human glutathione transferase P1-1. Crystallographic and kinetic studies on the Y108F mutant enzyme†,‡. *Biochemistry* **36**(20), 6207–6217. https://doi.org/10.1021/BI962813Z (1997).
86. Rosen, L. S. et al. Phase 1 study of TLK286 (telcyta) administered weekly in advanced malignancies. *Clin. Cancer Res.* **10**(11), 3689–3698. https://doi.org/10.1158/1078-0432.CCR-03-0687 (2004).
87. Kavanagh, J. J. et al. Multi-institutional phase 2 study of TLK286 (TELCYTA™, a glutathione S-transferase P1-1 activated glutathione analog prodrug) in patients with platinum and paclitaxel refractory or resistant ovarian cancer. *Int. J. Gynecol. Cancer* **15**(4), 593–600. https://doi.org/10.1136/ijgc-00009577-200507000-00003 (2005).
88. Vergote, I. et al. Phase 3 randomised study of canfosfamide (Telcyta®, TLK286) versus pegylated liposomal doxorubicin or topotecan as third-line therapy in patients with platinum-refractory or -resistant ovarian cancer. *Eur. J. Cancer* **45**(13), 2324–2332. https://doi.org/10.1016/j.ejca.2009.05.016 (2009).
89. Raza, A. et al. Phase 1 multicenter dose-escalation study of ezatiostat hydrochloride (TLK199 tablets), a novel glutathione analog prodrug, in patients with myelodysplastic syndrome. *Blood* **113** (26), 6533–6540. https://doi.org/10.1182/BLOOD-2009-01-176032 (2009).
90. Raza, A. et al. Phase 1-2a multicenter dose-escalation study of ezatiostat hydrochloride liposomes for injection (Telintra, TLK199), a novel glutathione analog prodrug in patients with myelodysplastic syndrome. *J. Hematol. Oncol.* https://doi.org/10.1186/1756-8722-2-20 (2009).

91. Raza, A. et al. A phase 2 randomized multicenter study of 2 extended dosing schedules of oral ezatiostat in low to intermediate-1 risk myelodysplastic syndrome. *Cancer* **118**(8), 2138–2147. https://doi.org/10.1002/CNCR.26469 (2012).
92. Search ClinicalTrials. gov for: Other terms: PF-03715455 | List Results | ClinicalTrials.gov. (accessed Dec. 02, 2025). https://clinicaltrials.gov/search?term=PF-03715455&viewType=Table (2025).
93. Ho-Yen, C. M., Jones, J. L. & Kermorgant, S. The clinical and functional significance of c-Met in breast cancer: A review. *Breast Cancer Res.* **17**(1), 52. https://doi.org/10.1186/S13058-015-0547-6 (2015).
94. Pérez-Ramírez, C., Cañadas-Garre, M., Molina, M. Á., Faus-Dáder, M. J. & Calleja-Hernández, M. Á. MET/HGF targeted drugs as potential therapeutic strategies in non-small cell lung cancer. *Pharmacol. Res.* **102**, 90–106. https://doi.org/10.1016/J.PHRS.2015.09.016 (2015).
95. Baladi, T., Abet, V. & Piguel, S. State-of-the-art of small molecule inhibitors of the TAM family: The point of view of the chemist. *Eur. J. Med. Chem.* **105**, 220–237. https://doi.org/10.1016/J.EJMECH.2015.10.003 (2015).
96. Zhu, C., Wei, Y. & Wei, X. AXL receptor tyrosine kinase as a promising anti-cancer approach: Functions, molecular mechanisms and clinical applications. *Mol. Cancer* **18**(1), 153. https://doi.org/10.1186/S12943-019-1090-3 (2019).
97. Robinson, J. et al. Investigating the impact of aromatic ring substitutions on selectivity for a multimodal anion exchange prototype library. *J. Chromatogr. A* **1569**, 101–109. https://doi.org/10.1016/J.CHROMA.2018.07.049 (2018).
98. Hedgethorne, K. & Huang, P. H. Foretinib: c-Met and VEGFR-2 inhibitor oncolytic. *Drugs Future* **35**(11), 893–901. https://doi.org/10.1358/DOF.2010.35.11.1529012 (2010).

Authors and Affiliations

Marouane Aherkou[1,2,3] · Mohammed Hakmi[2,3] · Yassir Boulaamane[4] · Azeddine Ibrahimi[1]

✉ Azeddine Ibrahimi
a.ibrahimi@um5r.ac.ma

[1] Medical Biotechnology Laboratory (MedBiotech), Bioinova Research Center, Faculty of Medicine and Pharmacy of Rabat, Mohammed V University, Rabat, Morocco

[2] Mohammed VI University of Sciences and Health (UM6SS), Casablanca, Morocco

[3] Mohammed VI Center for Research and Innovation (CM6RI), Rabat, Morocco

[4] Laboratory of Innovative Technologies, National School of Applied Sciences of Tangier, Abdelmalek Essaadi University, Tetouan, Morocco